Journal of Solid State Chemistry **161,** 73–79 (2001)
doi:10.1006/jssc.2001.9269, available online at http://www.idealibrary.com on IDEAL®

Theoretical Approach to Ionic Conductivity in Phosphorus Oxynitride Compounds

Hassan Rabaâ,*,[1] Roald Hoffmann,†,[1] Norge Cruz Hernández,‡ and Javier Fernandez Sanz‡

*Département de Chimie, Université Ibn Tofail, L.C.T.A., P.O. Box 133, 14000 Kénitra, Morocco; †Department of Chemistry and Chemical Biology, Cornell University, Ithaca, New York, 14853-1301; and ‡Departamento de Química Física, L.Q.F., Facultad de Química, E-41012 Sevilla, Spain

Received October 13, 2000; in revised form March 7, 2001; accepted June 8, 2001; published online August 22, 2001

B3YLP density functional calculations have been performed to study the ionic conductivity in γ-Li_3PO_4 and γ-$Li_{2.88}PO_{3.73}N_{0.14}$. Starting from the crystal structure of γ-$Li_{2.88}PO_{3.73}N_{0.14}$, we construct a model cluster without defects, $Li_{15}PO_{10}$, as well as another new oxynitride, $Li_{14}PO_8N$, in which lithium and oxygen defects are introduced as one oxygen is substituted by nitrogen. To model the ionic conductivity in these materials, different pathways of lithium motion are considered. The first one involves a Li^+ motion between two crystallographic sites through faces of adjacent LiO_4 tetrahedron via an unoccupied octahedral site. The second one involves a direct Li^+ motion through faces of adjacent LiO_4 tetrahedra. Both mechanisms are unlikely for the parent model cluster because of the high computed energy barrier associated with Li^+ mobility in the cluster. In contrast, we obtain a reasonable energy barrier in the nitride cluster which has Li^+ and O^{2-} defects creation and incorporates nitrogen. The barrier was computed to be about 1.26 eV for Li^+ mobility through tetrahedral faces for the nitride structure, compared to 4.8 eV in the parent cluster. Considering parameters such as Li–N covalency, ionic radius, and tetrahedral distortion, the nitridation could be expected to enhance the ionic conductivity. We connect the magnitude of the ionic conductivity to the height of the energy barrier computed for Li^+ jumping between different crystallographic sites. © 2001 Academic Press

Key Words: **γ-Li_3PO_4 and γ-$Li_{2.88}PO_{3.73}N_{0.14}$; cluster models; ionic conductivity; lithium mobility.**

INTRODUCTION

High lithium ion conductivity in lithium phosphorus oxynitride has been the subject of many recent investigations (1–7). Many phosphorus oxynitride electrolytes incorporate a remarkable amount of lithium and have been considered for possible application in rechargeable thin-film lithium batteries (4). Inclusion of nitrogen in the structure of amorphous lithium phosphate thin films increases the lithium ion conductivity. Recently, Wang *et al.* (5) have reported a neutron diffraction study of crystalline lithium phosphorous oxynitrides of γ-Li_3PO_4 (**A**) and the nitrogen-doped defect phase γ-$Li_{2.88}PO_{3.73}N_{0.14}$ (**B**), and have investigated the structural effect of nitrogen doping on ionic conductivity.

The purpose of this work is to analyze theoretically the energy barrier for Li^+ ion transport in these materials. Our strategy involves construction of a model cluster without defects from the crystallographic structure of **B**, $Li_{15}PO_{10}$, as well as a nitride $Li_{14}PO_8N$ cluster with simulated defects. We examine the relationship between structures and properties in these compounds and compute the energy barriers related to lithium mobility in the cluster models, thereby connecting ionic conductivity with the physical process of Li^+ ion jumping between different crystallographic sites.

CLUSTER MODELS

Let us recall briefly the crystal structure of γ-Li_3PO_4 (5–9, 12). In Scheme 1, we show a portion of structure **A**. In it there are two types of lithium atoms (Li_I and Li_{II}) and three types of oxygen (O_I, O_{II}, and O_{III}). We observe also that each $Li_{II}O_4$ tetrahedron shares adjacent edges with two Li_IO_4 tetrahedra, which in turn share only corners with other Li_IO_4 tetrahedra. The phosphorus atom is omitted in this partial view.

Figure 1 shows the γ-Li_3PO_4 structure (**A**). Each oxygen is shared by three LiO_4 tetrahedra and one PO_4 tetrahedron. The major peculiarity seen in this structure is some edge sharing of LiO_4 tetrahedra which does not exist in other varieties such as α- and β-Li_3PO_4.

The unit cell volumes of **A** and **B** are close to each other; with $Z = 4$, six atoms occupy the asymmetric unit: three tetrahedral cations (Li_I, Li_{II}, and P). From the X-ray data (5), we note some differences and similarities between the parent (**A**) and the nitrided (**B**) structures (Table 1).

[1]To whom correspondence should be addressed. Fax: (607) 255-5707. E-mail: rh34@cornell.edu or hrabaa@yahoo.com.

0022-4596/01 $35.00

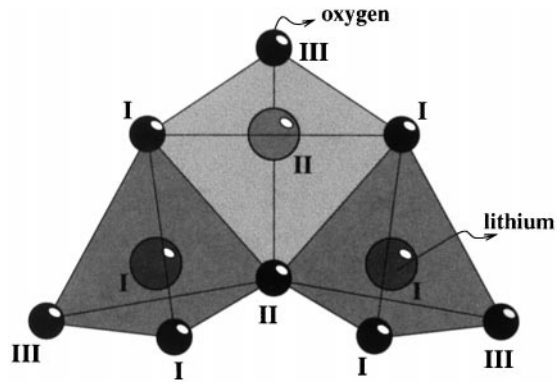

SCHEME 1. A partial structure of γ-Li_3PO_4, showing edge sharing of two Li_IO_4 tetrahedra with one $Li_{II}O_4$. The Li_IO_4 and $Li_{II}O_4$ tetrahedra are further distinguished by dark and light shading. The small circles are oxygen atoms; the big ones are lithiums. The light tetrahedron contains lithium(II) atoms and the dark tetrahedra lithium(I).

There are substantial perturbations in the bond distances and angles upon incorporation of nitrogen in the lattice, in both P and Li tetrahedra. By adding nitrogen to the lattice, some P–O distances are lengthened from 1.55 Å to 1.58 Å, while others are shortened from 1.53 Å to 1.49 Å. Even the Li–O distances are affected, and the variations in O–Li–O angles are also significant. The bond valence parameters of Brown and Altermatt (10) applied to this material confirm these changes and indicate that the O_{II} and O_{III} distances to lithium are substantially affected by the introduction of nitrogen.

The above-quoted experimental study also finds that the incorporation of a small amount of nitrogen in the lattice increases the ionic conductivity by several orders of magnitude (5).

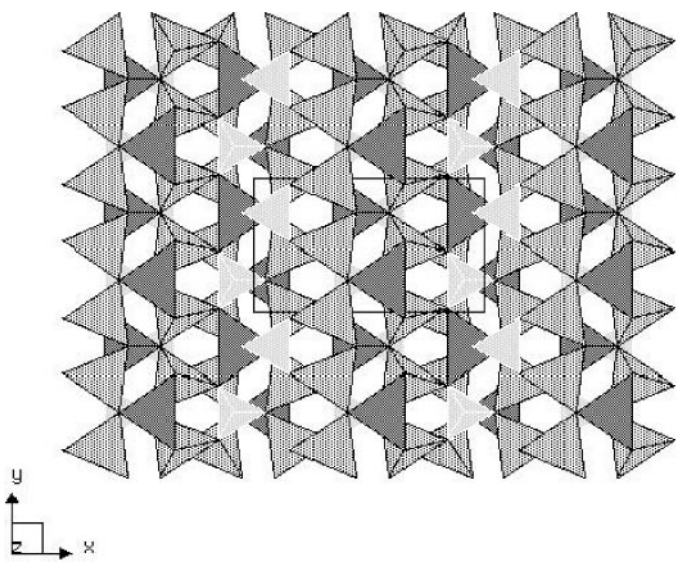

FIG. 1. Polyhedral crystal structure view along (001) of γ-Li_3PO_4. The lighter shaded tetrahedra are PO_4. The Li_IO_4 and $Li_{II}O_4$ tetrahedra are further distinguished by dark and gray shading, respectively.

TABLE 1
Selected Interatomic Distances (Å), Angles (°), and Standard Deviations for γ-Li_3PO_4 and $Li_{2.88}PO_{3.73}N_{0.14}$ from Ref. (5)

	γ-Li_3PO_4 (**A**)	$Li_{2.88}PO_{3.73}N_{0.14}$ (**B**)
	PO_4 Tetrahedron	
$P–O_I$	1.539(1)	1.538(5)
$P–O_I$	1.539(1)	1.538(5)
$P–O_{II}$	1.533(2)	1.497(8)
$P–O_{III}$	1.547(2)	1.583(7)
$O_I–P–O_I$	109.6(1)	111.4(4)
$O_I–P–O_{II}$	110.0(8)	112.5(2)
$O_I–P–O_{III}$	112.5(2)	108.8(8)
	Li_IO_4 Tetrahedron	
$Li_I–O_I$	1.951(3)	2.001(1)
$Li_I–O_{II}$	1.936(3)	1.886(1)
$Li_I–O_{III}$	1.913(3)	1.936(1)
$O_I–Li_I–O_I$	106.2(1)	105.1(5)
$O_I–Li_I–O_{II}$	96.2(1)	101.2(6)
	$Li_{II}O_4$ Tetrahedron	
$Li_{II}–O_I$	1.995(2)	1.974(7)
$Li_{II}–O_{II}$	2.043(5)	2.106(1)
$Li_{II}–O_{III}$	1.926(4)	1.944(1)
$O_I–Li_{II}–O_I$	128.5(2)	129.5(8)
$O_I–Li_{II}–O_{II}$	93.3(1)	95.0(5)

Let us examine both cluster models used in this theoretical investigation. The material we wish to study is a nonstoichiometric compound γ-$Li_{2.88}PO_{3.73}N_{0.14}$ (**B**). Starting from the unit cell crystallographic data of **B** without any nitrogen or defects ($Li_{12}P_4O_{16}$), we built a first model cluster $Li_{15}PO_{10}$ (**C**) (Scheme 2).

To reduce the computational cost, we decided to work with such a small cluster (**C**), constructed by omitting three phosphorus tetrahedra. The cluster that remains contains three edge-sharing tetrahedra of lithium taken from the unit cell in the crystal structure of **B**, two of them sharing vertices with PO_4 tetrahedron. Cluster neutrality is necessary for the calculations, so we "saturate" **C** by adding some lithium ions, keeping the same crystallographic positions as in **B**. Schemes 1 and 2 illustrate the same cluster structure of **C**; the difference is that in Scheme 1 we omit a PO_4 tetrahedron for clarity.

In Scheme 3, we show four steps in the construction of cluster models (**C**, **D**, **E**, and **F**) by removing and substituting atoms from **B**. In the first step, we begin from the idealized cluster ($Li_{15}PO_{10}$, **C**). We next build a cluster model ($(Li_{15}PO_9N)^{-1}$, **D**) by substituting one oxygen by nitrogen. There are three types of oxygen (O_I, O_{II}, or O_{III}) that could be substituted by nitrogen. To account for the structural defects upon nitrogen incorporation in **C**, we used

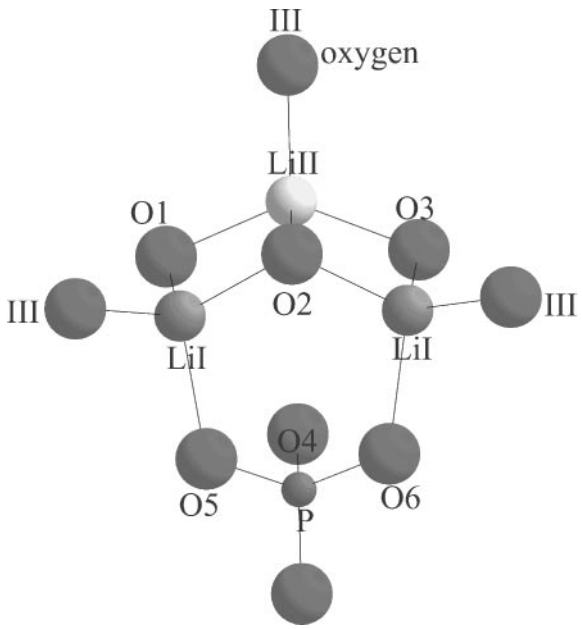

SCHEME 2. A partial structure model cluster of ($Li_{15}PO_{10}$) (**C**), showing edge sharing of two Li_IO_4 with one $Li_{II}O_4$ and one PO_4 tetrahedra. For scheme clarity, we omit the 12 lithium atoms which surround the shown cluster (arabic numerals indicate specifically the unoccupied hexacoordinate Li position).

charge and valence considerations (11, 12). The charge distribution argues for replacement of the most positive oxygen (O_{II}) by nitrogen. Extended Hückel (EH) (13) and B3LYP calculations show a relative stabilization energy of nearly 0.15 eV when we substitute O_{II} (instead of O_I or O_{III}) by nitrogen (see Scheme 3). This substitution leads to **D** in Scheme 3.

We next constructed model **E**, $(Li_{14}PO_9N)^{-2}$, a model for a lithium defect. We were guided by Pauling's rules for an ionic solid (12) in choosing which lithium (Li_I, Li_{II}) to remove. To construct **E** from **D**, one should minimize the cation–cation repulsion inside the cluster. The best candidate lithium atom to be removed is Li_{II}, rather than Li_I, and indeed this leads to greater computed stability (calculated as over 0.3 eV in B3LYP calculations) in **E**.

We next want to remove one oxide ion from **E** to obtain a neutral ($Li_{14}PO_9N$, **F**). B3LYP calculations show a relative stabilization energy of **F** about 0.33 eV upon removing oxygen O_{III} instead of O_{II} or O_I near the incoming nitrogen. The computed total energy difference between placing the Li(II) ion near and far away from the incoming nitrogen is 0.25 eV, which led us to opt for putting the Li ion near the nitrogen atom in **F**.

To summarize, the substitution and the removal of atoms as one moves from **C** to **F** may be described as a concentration of lithium defects close to the incoming nitrogen (13). Using our model we can assign the short Li_I–O_{II} bond distance to the Li_I–N bond. This agrees with what we have seen happen in the crystal structure when we introduce nitrogen into the lattice (Table 1). Also, the previous EH calculations performed on the extended structure of **A** and **B** (13), concluding on the basis of the charge distribution

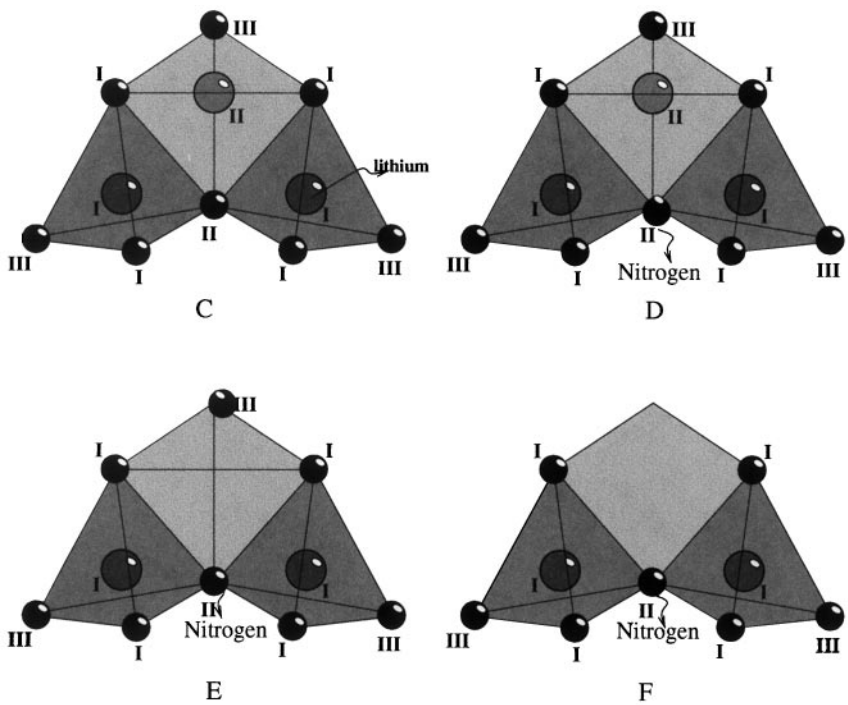

SCHEME 3. Four steps in constructing the model clusters: (**C**) the starting point, all atoms in the block retained; (**D**) nitrogen substituted in the O_{II} position; (**E**) a vacancy created in the Li_{II} position; (**F**) oxygen is removed from the O_{III} position.

that the O_{II} should be substituted by nitrogen for example, agree with this substitution.

COMPUTATIONAL DETAILS

B3YLP density functional calculations of the electronic structure of the various molecular models studies were carried out with the Gaussian 94 package (14–16), using a double-zeta 6-31G basis set for phosphorus (17), oxygen, and each of the three lithium atoms located in the center of this cluster. The lithium ions surrounding the cluster **C** are described only by a minimal basis (STO-3G). The initial geometry was based on the crystal structure (5); we then optimized the geometry of the three important lithiums (two Li_I and one Li_{II}) in the center of each model cluster.

Two kinds of lithium pathways through clusters **C** and **F** are investigated for modeling the Li^+ ion mobility.

Pathway 1: We show in Scheme 4 the model cluster **C**, in which we have three edge-sharing tetrahedra of lithium, which share vertices with PO_4 tetrahedron (see Scheme 4). One can see that there is an unoccupied site, approximately in the center of these four tetrahedra. This "octahedral" site (marked by a lined circle in Scheme 4) is surrounded by six neighboring oxygen atoms (O_1–O_6) (Arabic numerals used as oxygen labels in Schemes 2 and 4 indicate specifically the unoccupied hexacoordinate Li position), and serves as an intermediate position along the reaction coordinate for pathway 1. Along this pathway, we use a hypothetical reaction coordinate based on a linear transit (straight line) between the starting point (i.e., Li_I) and the octahedral site. This is followed by another linear transit between this midpoint and the Li_{II} vacant site.

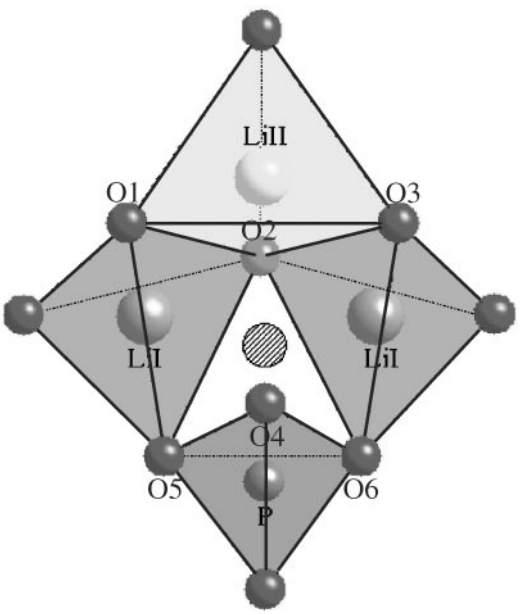

SCHEME 4. A set of three adjacent LiO_4 tetrahedra, two of which (Li_I) share vertices with PO_4 tetrahedra in the γ-Li_3PO_4 structure. The dark circles are oxygen atoms; the light circles are lithium atoms. The lined circle marks the center of the unoccupied octahedral site surrounded by the six oxygen atoms, O_1–O_6.

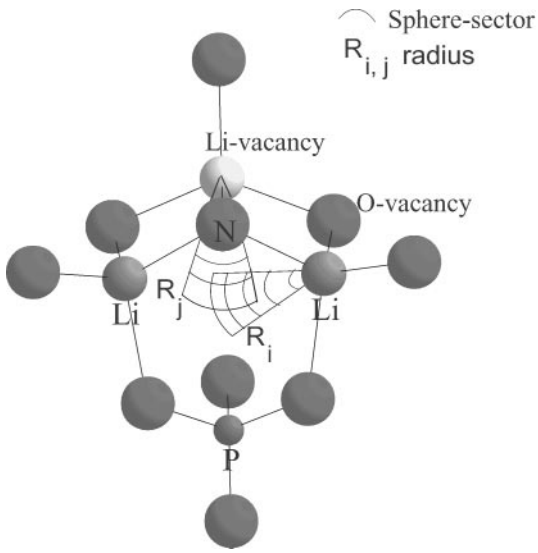

SCHEME 5. Two sphere sectors each centered in one interstitial site (i.e., Li_I and Li_{II} atoms).

Pathway 2: We use a second, different hypothetical reaction coordinate. This involves a direct Li^+ motion through faces of LiO_4 tetrahedra, from an occupied site (i.e., Li_I) to another neighbor vacant site (i.e., Li_{II}) inside the cluster. Let us describe this second pathway in some detail.

Inclusion of a defect decreases the steric effects inside the cluster and leads to greater lithium mobility in **F** than in **C**. So, to allow one lithium mobility, we decide to use two spherical sectors centered on the center of two adjacent LiO_4 tetrahedra. These two sphere sectors impose boundaries on the allowed motion of the Li^+ ion. We divide each sphere sector in several equal regions (portion). Each region corresponds to a particular sphere radius (see Scheme 5), measured from the specified Li^+ ion position. In each region we explored the energy of many different but closely related structures. We systematically moved the Li^+ ion from one region (R_i) to the next region (R_{i+1}) within the first spherical sector, until it overlaps with the second spherical sector, one centered on the Li_{II} unoccupied position. Similar calculations were then performed in the second sphere sector. The reaction coordinate for Li^+ diffusion is defined as a smooth curve that connects the lowest energy structure in each region.

RESULT AND DISCUSSION

1. Barrier Energy

Let us compare the possibilities for Li^+ motion in **A** and **B**. In the parent structure **A**, the Li^+ ions occupy tetrahedral

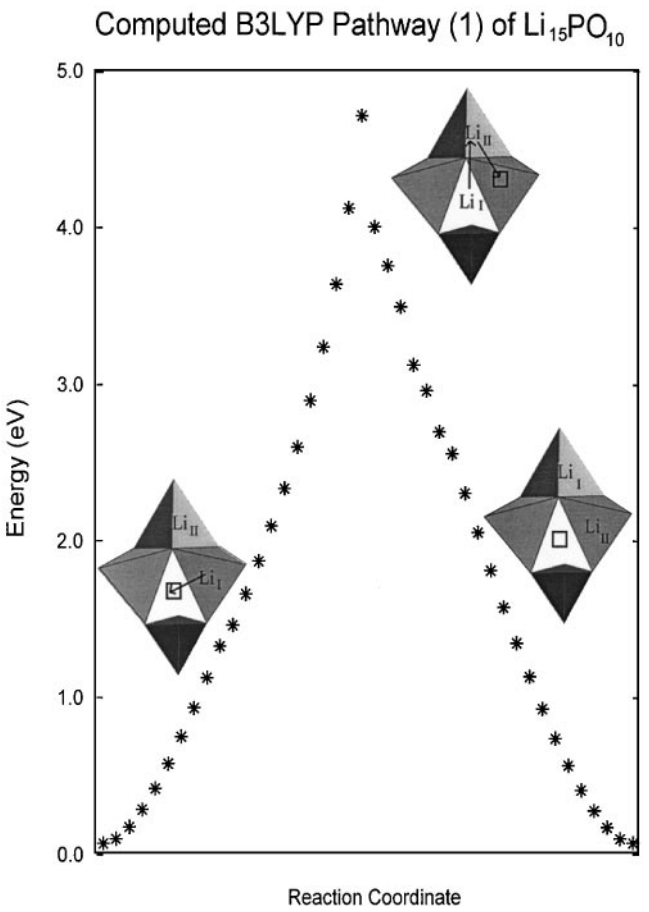

FIG. 2. Two curves illustrating the first pathway in $Li_{15}PO_{10}$. The left one concerns the straight-line lithium mobility between the center of the Li_IO_4 tetrahedron and the octahedral site. The right one shows the lithium mobility between the octahedral site and the center of the $Li_{II}O_4$ tetrahedron.

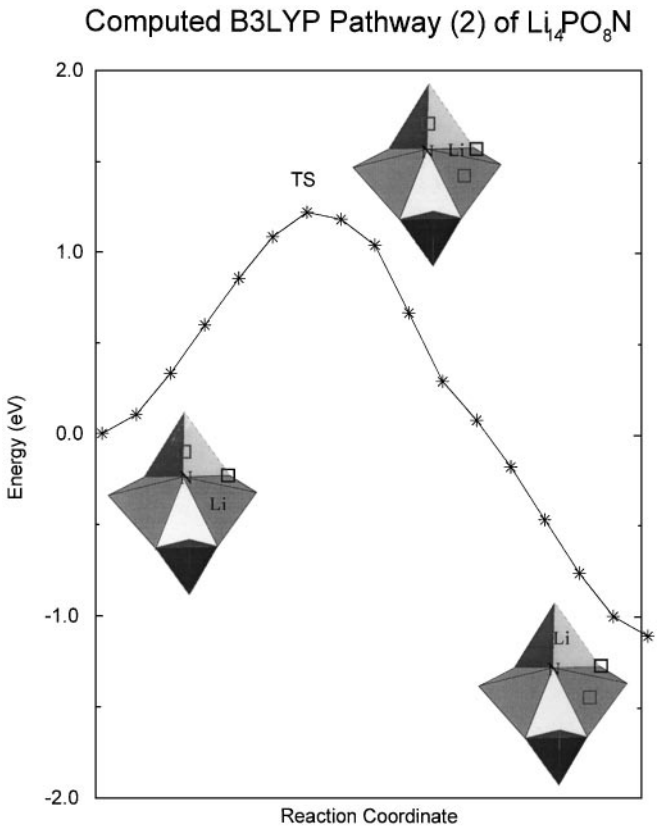

FIG. 3. Computed energy of the Li^+ ion crossing tetrahedral faces in $Li_{14}PO_8N$. The lithium moves from the center of the Li_IO_4 tetrahedron until the transition state, and then moves to the center of the $Li_{II}O_4$ tetrahedron.

sites in a framework structure formed by the P and O, and all Li sites are fully occupied. On the other hand, in γ-$Li_{2.88}PO_{3.73}N_{0.14}$ (**B**) a large concentration of vacancies is available. In addition, the replacement of smaller O^{2-} ions by larger N^{3-} ions increases the size of the small bottleneck through which the lithium ions must pass in **B**. In fact, we expect that the presence of such a vacant site should facilitate the jumping of Li^+ ions between various lithium positions in **A** and should explain also the lower ionic conductivity of lithium. An octahedral site may contribute to Li^+ motion, but whether it does or not depends on the height of the energy barrier along the reaction coordinate.

We proceed to evaluate the energy barrier to Li^+ mobility in clusters **C** and **F** by the first pathway. Figure 2 shows the result for **C**. In this figure we have two curve portions: the left one describes the first Li^+ motion from the Li_I site to the octahedral site; the right one corresponds to the second motion of Li^+ from the same octahedral site to a second position Li_{II}. To avoid cation–cation repulsion of Li_I and Li_{II} during the second portion of lithium migration, we moved Li_{II} and Li_I simultaneously. Thus, as the Li_I continues its motion (top of the second curve portion in Fig. 2) from the octahedral site to the next site, we move the second Li_{II} across a face to the other unoccupied site. The intersection of the two curves is taken as an estimate of the energy barrier for this reaction coordinate.

In fact, we find a high barrier energy for **C** in the first pathway, equal to 4.8 eV. This is to be compared to 2.6 eV for **F** computed in the same way. We attribute this high energy barrier encountered in **C** to the difficult migration of lithium from stable tetrahedral coordination to an unstable "octahedral" site. By analyzing the wave function, we find that the energy barrier is not related to an avoided crossing or core–core Li–Li repulsion.

Along this reaction coordinate for **C**, the lithium atom leaves a stable tetracoordination of LiO_4, and crosses a tricoordinate environment LiO_3 (i.e., in the first face), finishing its jump in an unstable coordination site (i.e., LiO_6) (see Scheme 4).

The crossing of faces during the lithium motion is not identical in **F** and in **C**, because inclusion of the defect

changes the space and the environment of Li^+ ions and contributes to easier lithium diffusion in **F**. The vacancy appears to be required to enhance the mobility of Li^+ in the net and should explain the lower barrier energy value found in **F**.

In **F** the presence of nitrogen better stabilizes the intermediate lithium position, presumably because of the greater effective ionic radius of N^{3-} (1.32 Å) than O^{2-} (1.24 Å). Additionally, the nitrogen orbital, which is more diffuse, contributes to the stabilization of the Li^+ ion during its jump, by forming a partially covalent Li–N bond. But in the octahedral site the Li–O bonds are still much longer (2.3 Å) and weakened.

Let us now consider the second lithium pathway. The computed energy barrier in **F** associated with the mobility of the Li^+ ion in this pathway is about 1.26 eV (Fig. 3).

As Fig. 3 shows, one possible transition state (TS) was found in the second reaction path of lithium motion. It was taken to be the middle point of the Li^+ ion trajectory.

So which pathway is the more probable? The two energy barriers in pathways 1 and 2 are quite different; we choose the second path, the one with the lower energy barrier. The second pathway may explain the greater diffusion and easier transport of Li^+ ions in oxynitride clusters.

2. *Ionic Conductivity*

We next link the ionic conductivity to the activation energy for Li^+ motion.

As reported in (5), compounds **A** and **B** obey the Arrhenius Eq. [1],

$$\sigma T = \sigma_0 \exp(-E_a/RT), \qquad [1]$$

in which σ_0 is the preexponential factor; E_a, activation energy; σ, the ionic conductivity; and T, temperature. The computed energy barrier should be this activation energy (E_a) (18).

From Figs. 2 and 3, one can see that the two curves do not have the same shape, and that the energy barrier is 4 times larger in **C** than in **F**. Incorporation of nitrogen gives a lower activation energy (E_a) in **F**. The addition of nitrogen and a defect is responsible for this large change, decreasing the energy barrier for lithium motion.

Let us consider the effect of nitridation on the ionic transport in these clusters (19, 20, 24). To produce a high mobility of lithium species in the lattice through tetrahedral faces, the lithium must cross faces rather than edges of LiO_4 tetrahedra. For example, in the structure of **A**, the oxygen–lithium distance for a lithium atom in the center of one face of a tetrahedron is 2.8 Å, but at the midpoint of an edge it is equal to 1.12 Å (assuming no displacement of O's). It is clear that the lithium ions will have less difficulty in crossing the face than the edge of the LiO_4 tetrahedron.

From the experimental data (5), we know that the ionic conductivity ($\sigma_{25°C}$) of **A** and **B** is equal respectively to 10^{-18} and 10^{-13} S.cm^{-1} ($\sigma_B/\sigma_A = 10^5$). The activation energies for γ-Li_3PO_4 and γ-$Li_{2.88}PO_{3.73}N_{0.14}$ (**A** and **B**) were calculated from experimental observations as 1.24 eV and 0.96 eV, respectively). The incorporation of a small amount of nitrogen in the lattice clearly increases the ionic conductivity by several orders of magnitude (5).

We note also a recent report on an oxynitride material ($Li_{0.99}PO_{2.55}N_{0.30}$) in which the authors found high conductivity of lithium and estimate the activation energy on nitridation to be equal to 0.6 eV (6). In other recent experimental work (17), the ionic conductivity of solid solutions of Li_3PO_4 and Li_4SiO_4 (comparing one to Li_3PO_4) was also attributed to a high vacancy concentration and cation substitution.

Let us focus on the ionic conductivity of Li^+ ion transport in our clusters **C** and **F**. In the conduction process, the Li^+ ions need to move through the solid. We find one possible pathway for Li^+ motion through faces of the LiO_4 tetrahedron, which can explain the conduction process. In our model, the computed energy barriers in **C** and **F** are 4.8 eV and 1.26 eV, respectively. We observe that the latter value is close to the experimental result (0.96 eV). So by injecting these calculated values as E_a in [1] we determine the ionic conductivity of **C** and F. Assuming the computed ionic conductivity (σ_C) and (σ_F), we calculated then the ratio of ionic conductivity (σ_F/σ_C) = 10^5, which gives the same order of σ in **A** and **B** ($\sigma_B/\sigma_A = 10^5$).

This work provides guidance in the choice of defect and nitrogen incorporation in order to decrease the activation energy in oxynitride compounds. We determine that two factors are promoters of this increase in the ionic conductivity: the lower energy barrier of Li^+ motion and creation defects of lithium and oxygen upon nitrogen incorporation.

SUMMARY

In this work we have constructed model clusters in order to study theoretically the relationship between the ionic conductivity and barrier energy in γ-Li_3PO_4 and its nitride variants. After a brief analysis of the model used for the calculation, we focused on the selectivity for different lithium pathways among the interstitial sites. By using various reaction coordinates related to the Li^+ motion, we explored the mobility of such ions. We have been able to estimate the energy barrier, with a preference found for a face–face migration pathway. The crucial differences between the two model clusters are the Li and O defects and nitrogen incorporation.

Our results indicate that the high ionic conductivity of the oxynitride compound is due to lower activation energy of Li^+ mobility in the defect lattice.

ACKNOWLEDGMENTS

The work at Cornell University was supported by the C.I.E.S. through a Fulbright Grant.

REFERENCES

1. J. B. Bates, G. R. Gruzalski, N. J. Dudney, C. F. Luck, X.-H. and S. D. Jones, *Solid State Technol.* July, **59** (1992).
2. J. B. Bates, G. R. Gruzalski, N. J. Dudney, R. H. Zuhr, A. Choudhury, C. F. Luck, and J. D. Roberston, *Solid State Ionics* **53,** 647 (1992).
3. A. Le Sauze, R. Marchand, and E. Gueguen, *J. Non-Cryst. Solids* **217,** 83 (1997).
4. M. R. Reidmeyer and D. E. Day, *J. Non-Cryst. Solids* **181,** 201 (1995).
5. B. Wang, B. C. Chakoumakos, B. C. Sales, B. S. Kwak, and J. Bates, *J. Solid State Chem.* **115,** 313 (1995).
6. B. Wang, B. C. Sales, B. S. Kwak, and J. B. Bates, *J. Non-Cryst. Solids* **183,** 297 (1995).
7. E. Reculeau, A. Elfakir, and M. Quarton, *J. Solid State Chem.* **79,** 205 (1989).
8. J. Zemann, *Acta Crystallogr.* **13,** 863 (1960).
9. R. D. Shannon, *Acta Crystallogr., Sect. A* **32,** 751 (1976).
10. I. D. Brown and D. Altermatt, *Acta Crystallogr., Sect. B* **24,** 244 (1985).
11. J. K. Burdett, *Acc. Chem. Res.* **15,** 34 (1982).
12. L. Pauling, "The nature of the Chemical Bond." Cornell Univ. Press, New York, 1960.
13. H. Rabaâ and R. Hoffmann, *J. Solid State Chem.* **145,** 619 (1999).
14. W. J. Stevens, H. Basch, and M. J. Krauss, *Chem. Phys.* **81,** 6062 (1984).
15. M. J. Frisch, G. W. Trucks, H. B. Schlegel, P. M. W. Gill, B. G. Johnson, M. A. Robb, J. R. Cheeseman, T. Keith, G. A. Petersson, K. Raghavachari, M. A. Al-Laham, V. G. Zakrzewski, J. V. Ortiz, J. B. Foresman, J. Cioslowski, B. B. Stefanov, A. Nanayakkara, M. Challacombe, C. Y. Peng, P. Y. Ayala, W. Chen, M. W. Wong, J. L. Kutzelnigg, J. L. Andres, E. S. Replogle, R. Gomperts, R. L. Martin, D. J. Fox, J. S. Binkley, D. J. Defrees, J. Baker, J. J. P. Stewart, M. Head-Gorden, C. Gonzalez, J. A. Pople, "Gaussian 94, Revision D2." Gaussian, Inc., Pittsburgh, PA, 1995.
16. A. D. Becke, *J. Chem. Phys.* **98,** 5648–5652 (1993); see also, C. Lee, W. Yang, and R. G. Parr, *Phys. Rev. B.* **37,** 785 (1988).
17. "Gaussian basis sets for Molecular Calculation" (S. Huzinaga, Ed.) Physical Science Data, 16. Elsevier, Amsterdam, 1984; T. H. Dunning, *in* "Modern Theoretical Chemistry" (H. F. Schaefer, III, Ed.), Vol. 2. Plenum, New York, 1977.
18. Y. W. Hu, I. D. Raistrick, and R. A. Huggins, *J. Electrochem. Soc.* **124,** 1240 (1977).
19. R. D. Shannon, B. E. Taylor, A. D. English, and T. Berzins, *Electrochim. Acta* **22,** 783 (1977).
20. B. Zhu and B. E. Mellander, *J. Chem. Mater. Res. Bull.* **28,** 321 (1995).
21. H. Y.-P. Hong, *Mater. Res. Bull.* **13,** 117 (1978).
22. G. Nuspl, K. Yoshizawa, and T. Yamabe, *J. Mater. Chem.* **7,** 2529 (1997).
23. T. Obura, N. Aoki, and T. Kanazawa, *J. Non-Cryst. Solids* **183,** 297 (1995).
24. W. H. Baur, *Inorg. Nucl. Chem. Lett.* **16,** 525 (1980).